Nonacethrene Unchained: A Cascade to Chiral Contorted Conjugated Hydrocarbon with Two sp³-Defects

Daniel Čavlović,[†] Daniel Häussinger,[‡] Olivier Blacque,[†] Prince Ravat,*[,‡,§] and Michal Juríček*[,†,‡]

[†]Department of Chemistry, University of Zurich, Winterthurerstrasse 190, 8057 Zurich, Switzerland

[‡]Department of Chemistry, University of Basel, St. Johanns-Ring 19, 4056 Basel, Switzerland

[§]Institute of Organic Chemistry, University of Würzburg, Am Hubland, 97074 Würzburg, Germany

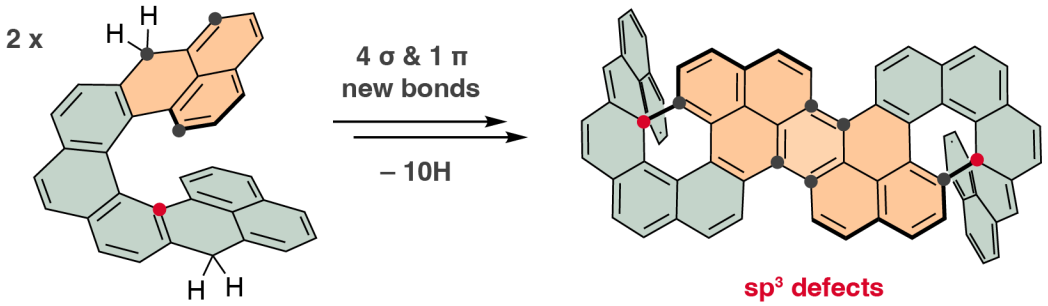

ABSTRACT: A dihydro precursor of helical diradicaloid nonacethrene undergoes a reaction cascade triggered by an oxidant to a chiral contorted polycyclic aromatic hydrocarbon named hypercethrene. In this ten-electron-oxidation process, four σ bonds, one π bond, and three six-membered rings are formed in a reaction sequence of up to nine steps to yield a 72-carbon-atom warped framework, comprising two configurationally locked [7]helicene units, fluorescent peropyrene unit, and two precisely installed sp³-defects. The key intermediate in this cascade is a closed nonacethrene derivative with one quaternary center, presumably formed via an electrocyclic ring closure of nonacethrene, which—when activated by oxidation—undergoes an oxidative dimerization of phenalenyl to peropyrene. By controlling the amount oxidant used, two intermediates and one side product could be isolated and fully characterized, including single-crystal X-ray diffraction analysis, and one intermediate was detected by electron paramagnetic resonance spectroscopy. In concert with density functional theory calculations, these intermediates support the proposed reaction mechanism. Compared to peropyrene, the absorption and emission of hypercethrene are slightly red-shifted on account of extended conjugation and the fluorescence quantum yield of 0.45 is decreased by a factor of ~2. Enantiomerically enriched hypercethrene displays circularly polarized luminescence with a CPL brightness value of 8.3 $M^{-1}cm^{-1}$. This unexpected reaction cascade demonstrates that the reactivity of "unchained" diradicaloid compounds, which is typically considered an undesired feature, can be well-defined and employed as a useful, step-economic synthetic tool toward novel carbon nanostructures.

INTRODUCTION

Polycyclic aromatic hydrocarbons (PAHs) with diradicaloid singlet ground state are investigated as molecular components of materials that display conductivity and magnetism[1−4]. These properties arise from two typical characteristics of diradicaloid compounds, namely, small HOMO–LUMO and small singlet–triplet (S–T) energy gap.[4−6] The diradical character of PAHs with a Kekulé electronic structure is achieved with quinoidal subunits, such as *ortho*- and *para*-quinodimethane (*o*-QDM and *p*-DQM, respectively), each unit stabilizing the diradical resonance structure of a PAH by one Clar's sextet. A large variety of Kekulé diradicaloids have been prepared by extending the structures of *o*-DQM and *p*-DQM. The classic as well as more recent examples—including Thiele's[7,8], Chichibabin's[8−10], and Müller's[11] hydrocarbons and their analogs[12], (peri)acenes[13,14], bis(phenalenyls)[15−17], indenofluorenes[18−20], sigmarene[21], zethrenes[22−24], and cethrenes[25,26]—demonstrate the versatility of molecular design and properties of PAHs with singlet diradical character.

The electronic structure of Kekulé diradicaloids is of interest also from another fundamental standpoint—reactivity—as illustrated[27] by the parent compounds *o*-DQM and *p*-DQM. Their reactivity is dual in nature, that is, it shows characteristics of closed-shell and open-shell systems. As an example, *o*-DQM undergoes thermal dimerization both via a concerted [4 + 2] cycloaddition mechanism as well as via a diradical mechanism yielding [4 + 4] cycloaddition dimer, which is formally a symmetry-forbidden process. Similar dual reactivity has recently been observed for sigmarene[21]. In the past, various aspects of reactivity of these and analogous systems were subject to extensive investigations.[6,28−30] In contrast, the current research is largely focused on the properties of extended diradicaloids, with efforts being made to suppress[17,30−32] their reactivity in order to obtain stable or persistent systems. A few recent reports indicate, however, that the reactivity of "unchained" diradicaloids, often

regarded as an undesired or a decomposition feature, can be utilized to create function[25,33−37], develop new methods[38,39], and deepen our chemical concepts[40,41].

Scheme 1. π-Radical Reactivity Overview[a]

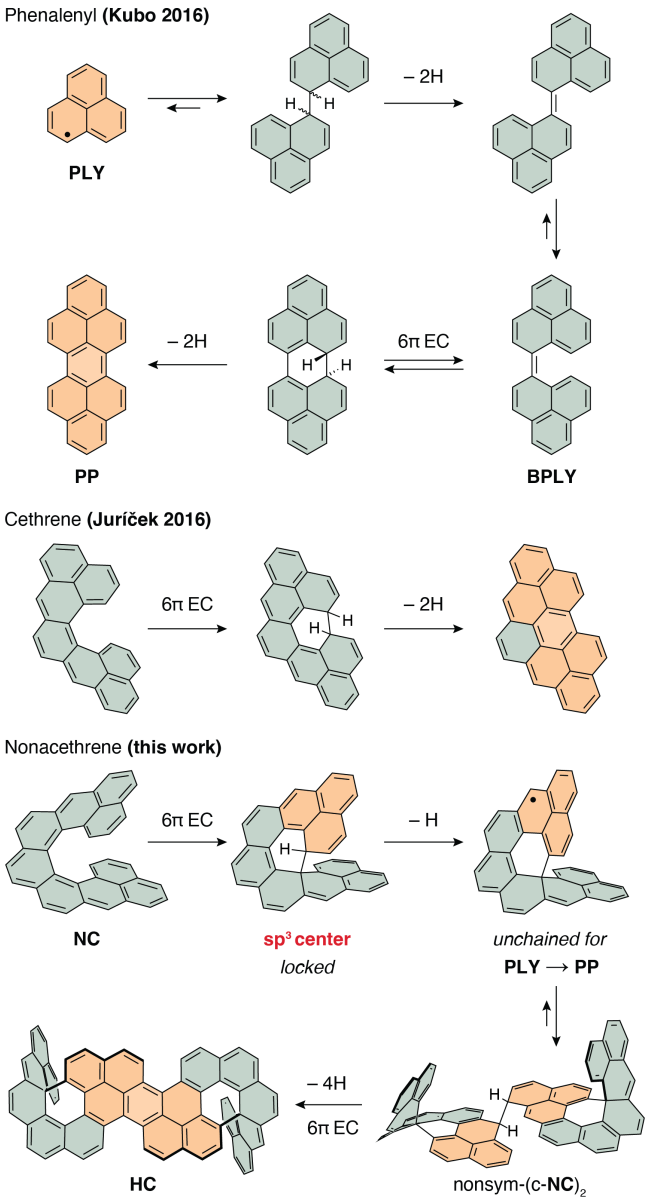

[a](Top) Decomposition pathway of phenalenyl (**PLY**) to peropyrene (**PP**) via 6π EC of biphenalenylidene (**BPLY**). (Middle) Cethrene's 6π EC followed by oxidation to a benzo-**PP** derivative. (Bottom) Nonacethrene's (**NC**) 6π EC "locks" the formed intermediate with a quaternary center (red). Upon oxidation, this intermediate is "unchained" for the **PLY**–**PP** cascade to hypercethrene (**HC**) over a nonsymmetric dimer (nonsym-(c-**NC**)$_2$).

Recent examples are biphenalenylidene (**BPLY**, Scheme 1, top), an intermediate on the decomposition pathway of phenalenyl (**PLY**) reported by Kubo et al.[28,42], and cethrene[26], a helical diradicaloid developed in our laboratory (Scheme 1, middle), which undergo a thermal 6π electrocyclization (EC). Even though this process is formally symmetry-forbidden in both compounds, it proceeds rapidly at temperatures below ambient as a result of small HOMO–LUMO gaps, and thus low-lying doubly excited states in **BPLY** and cethrene, which contributes to the lowering of the activation energies.

Using a dimethyl derivative of cethrene, in which the methyl groups prevent the oxidation to a flat hydrocarbon as observed for parent cethrene (Scheme 1, middle), we conceptualized[25] the working principle of a magnetic photoswitch that could be transformed reversibly between a magnetically active diradicaloid form and a magnetically inactive closed-shell form by light. Because the S–T gap of dimethylcethrene turned out to be too high to observe an electron paramagnetic resonance (EPR) signal at room temperature,[43] an extension of the helical backbone by two rings—to give nonacethrene (**NC**)—would overcome two challenges at once. First, the π-extended structure of **NC** should possess a significantly lower S–T gap enabling the detection of an EPR signal. Second, after the 6π EC ring closure, oxidation to a flat hydrocarbon as in the case of cethrene is not possible because the EC closure results in one quaternary center that "locks" the closed **NC** intermediate against oxidation of the formed σ bond (Scheme 1, bottom). Contrary to our expectations, the closed intermediate could not be isolated or detected because it readily oxidizes to a radical that is poised to undergo the **PLY**-to-**PP** transformation. Here, we present the study of this unexpected reaction cascade, including mechanistic insights and characterization of two intermediates and the extraordinary final product, a chiral contorted conjugated hydrocarbon with two sp^3-defects, named hypercethrene (**HC**; Scheme 1 and Scheme 3, bottom).

RESULTS AND DISCUSSION

Synthesis. The dihydro precursor of **NC**, 2*H*-**NC**, was synthesized starting from commercially available **1** (Scheme 1). Alternatively, **1** can be freshly prepared in one step as described in the literature[44,45]. The first step toward 2*H*-**NC** is a photocyclodehydrogenation of **1** to obtain 3,7-dibromophenanthrene (**2**) in >78% yield, which can be performed at high concentrations (>2 mM) due to the high photostability of the starting material and the product. In the next step, a two-fold lithium–halogen exchange[46] followed by a formylation gave after aqueous acidic workup dialdehyde **3** in >99% yield. Then, a Wittig reaction afforded an isomeric mixture[47] of **4**, which was subjected to another two-fold photocyclodehydrogenation to a yield helicene **5** in 62% yield over the two steps. The ester moieties in **5** were hydrolyzed under basic conditions to a give a diacid intermediate, which was transformed into the corresponding acyl chloride intermediate. Subsequent intramolecular Friedel–Crafts acylation with $TiCl_4$[48] resulted in diketone **6** in >99% yield over the three steps. Finally, reduction with sodium borohydride and elimination of water with *para*-toluenesulfonic acid yielded the dihydro precursor 2*H*-**NC** in 85% yield over the two steps. As observed before for analogous systems,[49] isomerization occurred during the dehydration step, where benzylic CH_2-groups migrated to give the most stable dihydro isomer featuring one phenanthrene and two naphthalene subunits. Enantiomerically enriched samples of (*P*)- and (*M*)-2*H*-**NC** were obtained from **6** resolved into enantiomers using HPLC equipped with a chiral stationary phase (Fig. S6–S8). The structure of 2*H*-**NC** was unambiguously confirmed by 1D and 2D NMR spectroscopy, with full assignment of proton and carbon resonances (Fig. 1 and Supplementary Information), HRMS, and single-crystal X-ray diffraction (SC-XRD) analysis of (*P*)-2*H*-**NC** (Fig. 2); the single crystals were obtained by slow evaporation of solvents from a solution of (*M*)-2*H*-**NC** in CH_2Cl_2 and hexanes.

Scheme 2. Synthesis of Dihydro Precursor of Nonacethrene (2*H*-NC) and its Oxidation to *O*-c-NC[a]

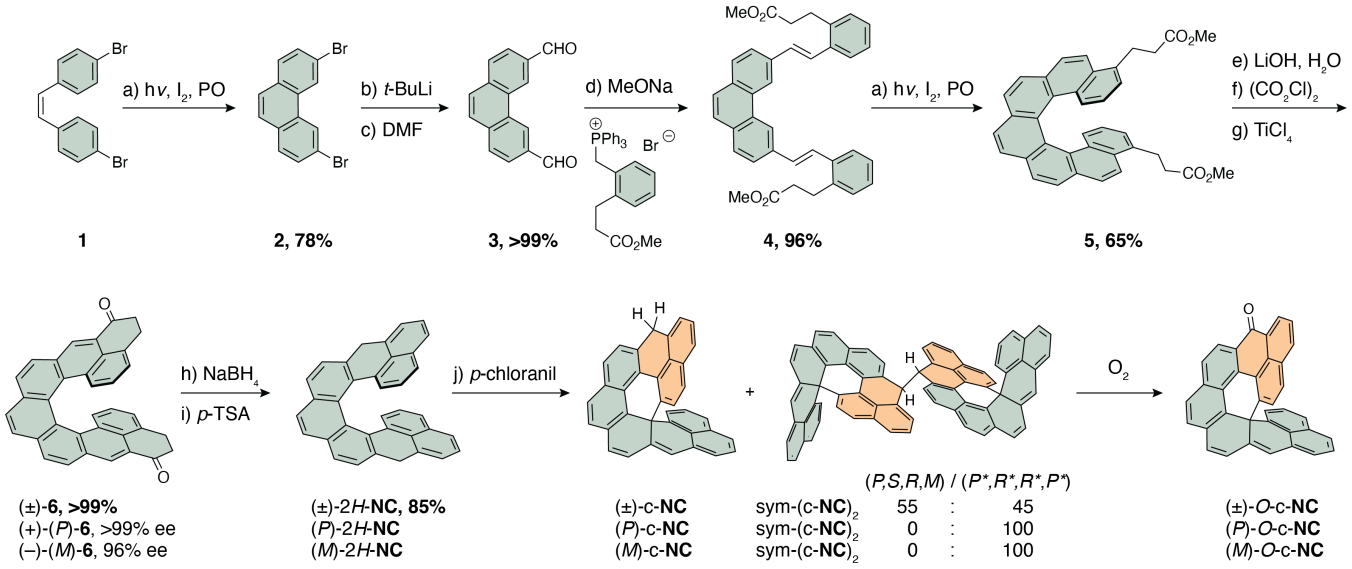

[a]Reaction conditions: (a) hν, I_2, propylene oxide, toluene, 20 °C, 14 h; (b) *t*-BuLi, THF, –78 °C, 0.5 h; (c) DMF, –78 °C to RT, 1 h; (d) MeONa, (2-(3-methoxy-3-oxopropyl)benzyl)triphenylphosphonium bromide, THF, RT, 12 h; (e) LiOH, THF/H_2O 10:1, reflux, 16 h; (f) $(CO_2Cl)_2$, 65 °C, 2 h; (g) $TiCl_4$, CH_2Cl_2, –40 to –25 °C, 5 h; (h) $NaBH_4$, CH_2Cl_2/EtOH 2:1, RT, 1 h; (i) *p*-TSA, toluene, 90 °C, 5 min; (j) *p*-chloranil, benzene-d_6, RT, 16 h. PO = propylene oxide, THF = tetrahydrofuran, DMF = *N*,*N*'-dimethyl formamide, RT = room temperature, *p*-TSA = *p*-toluenesulfonic acid.

With the aim to obtain **NC**, final oxidation under oxygen-free conditions with *p*-chloranil was performed. Unexpectedly, a variety of compounds formed and their relative ratio was dependent on the reaction time and the amount of oxidant used. Initially, c-**NC**, (c-**NC**)$_2$, and *O*-c-**NC** (Scheme 2) were identified, but further experiments revealed additional species, including **HC** (Scheme 3).

Oxidation Studies. Discovering the complex reactivity of the system, a systematic study of the oxidation process was carried out, varying the amount of oxidant used. In this set of experiments, either 0.5, 1, 1.5, 2, 2.5, 3 or 3.5 equivalents of oxidant were added to a solution of 2*H*-**NC** in benzene-d_6 (c ~ 7 mM) by using 50 mM solution of *p*-chloranil (CA) in benzene-d_6, all solutions being argon-saturated. The reaction progress was monitored in time by ^{1}H NMR spectroscopy, which revealed the composition of the reaction mixture at different stages. The individual oxidation experiments were compared, when significant changes were no longer occurring over time (Fig. 1).

Upon the addition of 0.5 equivalents of oxidant, two major species were observed in addition to the starting material 2*H*-**NC**. These species were identified as c-**NC**, a product of the apparent EC of **NC** followed by a hydrogen shift, and (c-**NC**)$_2$, a σ-dimer of oxidized c-**NC** (Scheme 2). With 1 equivalent of CA, 2*H*-**NC** was fully consumed and only c-**NC** and (c-**NC**)$_2$ were present, and with 1.5 equivalent of CA, only (c-**NC**)$_2$ was present as major species. All experiments exceeding 1.5 equivalents of oxidant lead to an unexpected outcome, formation of a new compound identified as **HC**. Recalling the findings of Kubo[42] and those from our laboratories[26][39], this result suggests further oxidation of the σ-dimer (c-**NC**)$_2$ followed by steps analogous to the **PLY**–**PP** cascade. In the conversion of 2*H*-**NC** to **HC**, overall four new σ-bonds and one new π-bond are formed, which is accompanied by a loss of ten hydrogen atoms (Scheme 1). Because CA is a two-electron oxidant, 3.5 equivalents of CA are required to achieve full conversion. In some experiments, a compound identified as *O*-c-**NC** (Scheme 2) was observed in varying amounts, even in experiments that were conducted under identical conditions. It was therefore rationalized that this product is formed due to trace amounts of oxygen present in the samples, which vary from sample to sample. Exposure of (c-**NC**)$_2$ to air resulted in a clean transformation to *O*-c-**NC** ultimately proving this assumption.

Structure Identification. To validate the structures of the observed intermediates c-**NC** and (c-**NC**)$_2$, side product *O*-c-**NC**, and final product **HC**, their proton and carbon resonances were all fully assigned by means of 2D NMR techniques, namely, COSY, TOCSY, NOESY/ROESY, HMQC/HSQC, and HMBC. For these measurements, c-**NC**, *O*-c-**NC**, and **HC** were isolated from the crude mixtures, when they formed in the highest quantities, depending on the amount of oxidant used (Fig. 1). Compound (c-**NC**)$_2$ was studied as formed when 1.5 equivalents of oxidant were used. An overview of the compounds and partial assignment of their proton resonances are shown in Figure 3. Full assignment of proton and carbon resonances is available in the Supplementary Information. The structures of (c-**NC**)$_2$ and *O*-c-**NC** were additionally confirmed by SC-XRD (Fig. 2).

The assignment for c-**NC** and *O*-c-**NC** was straightforward. It was used to identify (c-**NC**)$_2$ and **HC** because of the similarity of the structures. In general, most of the characteristic carbon shifts were not influenced significantly by the structural changes. The most characteristic shifts were those of the newly formed quaternary sp^3 carbon atom (50.1 ppm for c-**NC**) and three of the four neighboring sp^2 carbon atoms that were quaternary already prior to the closure (134.3, 136.4, and 143.6 ppm for c-**NC**). When comparing the ^{1}H NMR spectrum of (c-**NC**)$_2$ to that of c-**NC**, the main difference was that there was only one sp^3-proton instead of two, suggesting a substituent attached to this carbon atom. HMBC showed a correlation between the sp^3 proton and the carbon atom attached directly to the sp^3 carbon atom, which indicated that a σ-dimer had formed.

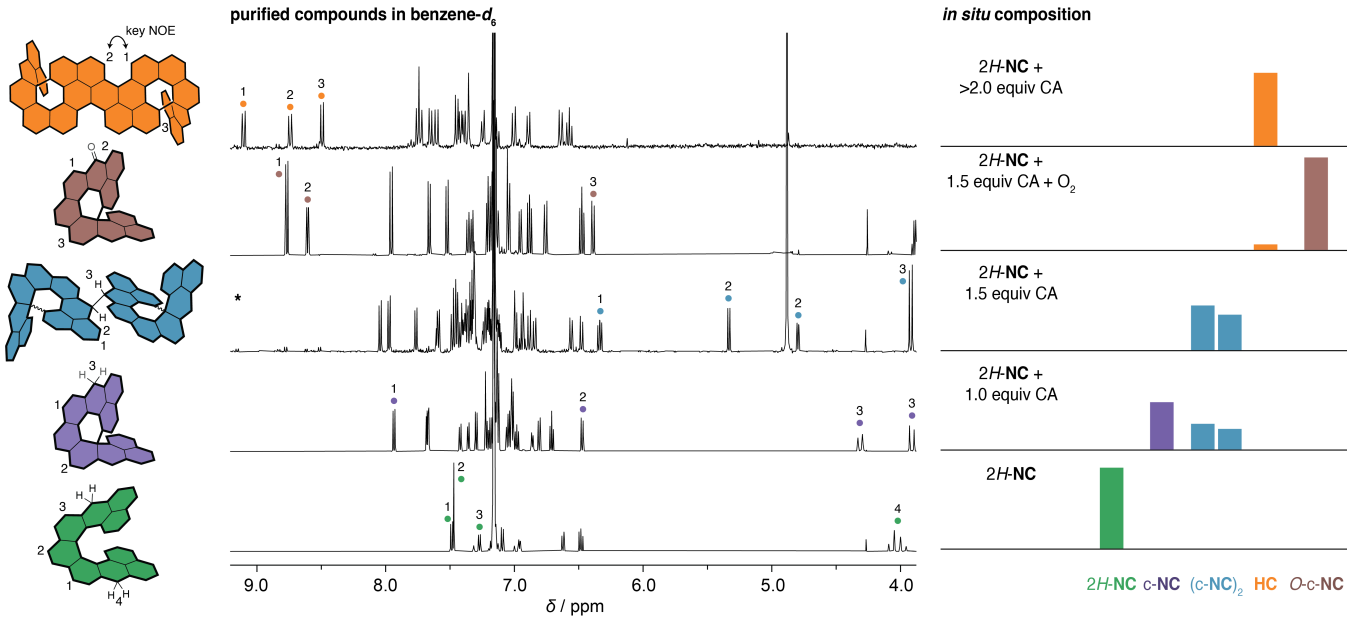

Figure 1. The ^{1}H NMR spectra of isolated, purified, and characterized compounds from the "unchained" reaction cascade with a partial assignment of the ^{1}H resonances. The amount of oxidant and the corresponding *in situ* composition is illustrated on the right. * Not purified. (c-**NC**)$_2$ resulted in a mixture of two diastereoisomers: sym-(*P**,*R**,*R**,*P**)-(c-**NC**)$_2$ and sym-(*P*,*S*,*R*,*M*)-(c-**NC**)$_2$. CA = *p*-chloranil.

The formation of the σ-dimer was further supported by the fact that two species with identical structure, but different chemical shifts (e.g., 3.93 and 3.90 ppm for the sp^3-proton) were present in a ratio 1:1.2. This observation indicates formation of two diastereomeric structures, which had to be symmetric because only one set of signals was observed for two monomeric units in each case. To identify the diastereomers, the oxidation experiment was repeated with enantiomerically enriched (*P*)- and (*M*)-2*H*-**NC** (*P* >99%ee; *M* 96%ee). In both cases, an identical spectrum was obtained (Figure S2), which means that the diastereomer with a singlet at 3.90 ppm had to be either sym-(*P*,*R*,*R*,*P*)-(c-**NC**)$_2$[50] or sym-(*M*,*S*,*S*,*M*)-(c-**NC**)$_2$, and the other diastereomer had to be achiral sym-(*P*,*S*,*R*,*M*)-(c-**NC**)$_2$. The structure of the achiral diastereomer was unambiguously confirmed by SC-XRD (Fig. 2).

For complete assignment (Fig. S24), the NMR spectra for **HC** were measured in tetrachloroethane-d_2 because of better solubility compared to benzene and no overlap with the solvent residual peak (Fig. S106–114). The key NOE correlation (Fig. S109) of the proton 1 and proton 2, unambiguously confirms the structure of **HC** and is depicted with an arrow in Scheme 3. This result was surprising, because this product cannot be formed from the observed symmetric σ-dimers sym-(c-**NC**)$_2$.

DFT Calculations. To shed light on the mechanism of this reaction cascade, DFT calculations were performed at the ωB97XD/Def2SVP level of theory (Scheme 3). The first detected, isolated, and characterized compound in the reaction cascade is c-**NC**. There are two reasonable pathways from 2*H*-**NC** to c-**NC**, both starting with oxidation of 2*H*-**NC** to *H*-**NC**·. From *H*-**NC**·, either a second oxidation takes place to give **NC**, which then undergoes EC to c-**NC***. Alternatively, *H*-**NC**· undergoes a radical ring closure to c-*H*-**NC**· and then oxidation to c-**NC***. By comparing optimized geometries of **NC**/c-**NC*** and *H*-**NC**·/c-*H*-**NC**·, both processes are thermodynamically favored (by 0.59 and 16.1 kcal mol^{-1}, respectively). In both cases, c-**NC*** isomerizes to c-**NC**, which is 6.78 kcal mol^{-1} more stable than c-**NC***.

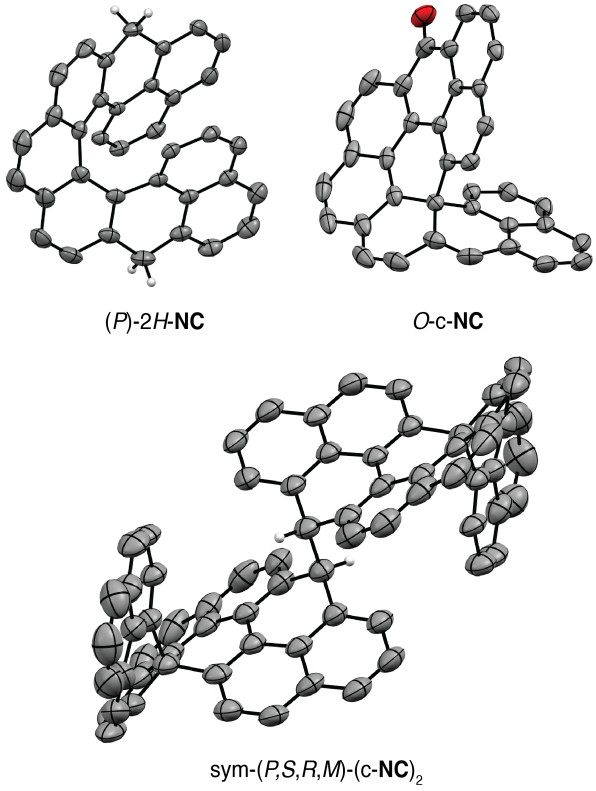

Figure 2. Perspective views of the solid-state structures of intermediates in the **NC** cascade from single-crystal X-ray diffraction analysis. The thermal ellipsoids are shown at the 50% probability level. Color code: C / gray, O / red, H / white. Most hydrogens are omitted for clarity.

Scheme 3. Proposed Mechanism for the Transformation of *H*-NC· to HC[a]

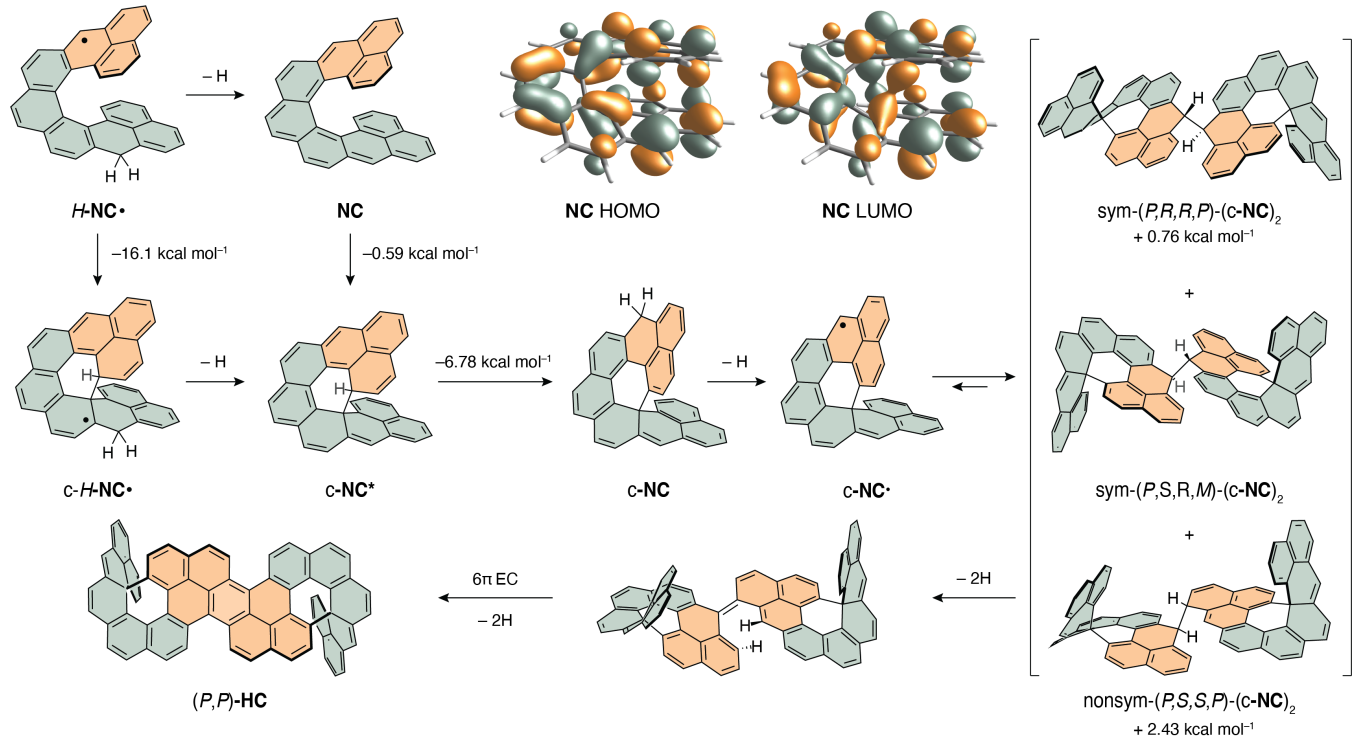

[a]Calculated relative energies (DFT/ ωB97XD/Def2SVP) are shown for isomeric structures.

c-**NC** then oxidizes to c-**NC**· (or c-**NC*** directly oxidizes to c-**NC**·), which is in equilibrium with several possible σ-dimers.[51] Analogous σ-dimerizations are well known in the literature[49,52,53]. Comparing the energies of sym-(*P**,*R**,*R**,*P**)-(c-**NC**)$_2$ relative to sym-(*P*,*R*,*S*,*M*)-(c-**NC**)$_2$, the difference in energy is only 0.76 kcal mol^{-1} which corroborates the observations in NMR. Based on the structure of **HC**, it is clear that **HC** must be formed from a nonsymmetric (c-**NC**)$_2$, that is, a dimer formed by linking two monomeric c-**NC**· units via different positions. The most stable, suitable non-symmetric dimer identified by DFT is non-sym-(*P**,*R**,*R**,*P**)-(c-**NC**)$_2$ (Tables S3 and S4), which is higher in energy by 1.67 and 2.43 kcal mol^{-1} when compared to sym-(*P**,*R**,*R**,*P**)-(c-**NC**)$_2$ and sym-(*P*,*R*,*S*,*M*)-(c-**NC**)$_2$ (Scheme 3).

Proposed Mechanism. The proposed mechanism for the 2*H*-**NC**–**HC** cascade is outlined in Scheme 3 and involves the formation of the first observable intermediate c-**NC**, its oxidation to c-**NC**·, which undergoes the **PLY**–**PP** cascade to form **HC**, the final product.

Initially, it was thought that c-**NC** is formed via 6π EC of **NC** and subsequent hydrogen shift. The reason for not observing **NC** as an intermediate could be a very low activation energy of EC due to **NC**'s small Singlet–Triplet gap (0.17 kcal mol^{-1}), which is significantly smaller than that of cethrene (5.6 kcal mol^{-1}).[26] Since the low-lying doubly excited state contributes to the lowering of the activation energy of this formally forbidden thermal process[41], EC of **NC** is expected to be much faster than that of cethrene (2× vs 1× antibonding interaction in the HOMO of **NC** vs cethrene; Scheme 3). Upon formation, **NC** would therefore immediately cyclize to c-**NC*** and not be detected. DFT calculations offer another possibility, namely, radical closure of mono-oxidized 2*H*-**NC**, *H*-**NC**·, and subsequent oxidation to c-**NC***. Based on calculations, both routes are plausible and none of them can be excluded. For isomerization of c-**NC*** to c-**NC**, a two-fold [1,3] or a [1,5] suprafacial sigmatropic hydrogen shift can be imagined as a mechanism for this hydrogen migration, in addition to acid-catalyzed isomerization (protons provided by reduced CA).

Oxidation of 2*H*-**NC** with 0.5 equivalent of CA (a two-electron oxidant) results in a mixture of 2*H*-**NC**, c-**NC**, and (c-**NC**)$_2$. This result indicates that formation of c-**NC** must be slower than its oxidation to c-**NC**·. Upon addition of 1 equivalent of CA, a significant amount of (c-**NC**)$_2$ was observed while 2*H*-**NC** was not present anymore (Fig. 1). Therefore, oxidation of (c-**NC**)$_2$ must be slower than oxidation of c-**NC** but faster than formation of c-**NC**. With 1.5 equivalents of CA, a point is reached where only (c-**NC**)$_2$ is observed.

The two observed (c-**NC**)$_2$ species are in equilibrium with the monomeric radical species, c-**NC**·. The presence of c-**NC**· was validated by EPR spectroscopy of a solution of (c-**NC**)$_2$, where the radical species could be detected even after two weeks of storing (c-**NC**)$_2$ in the glovebox (Fig. 3). A higher signal intensity could not be achieved as the equilibrium is largely shifted toward the dimer. The simulated EPR spectrum reproduces well the main features of the experimental one, and the proton hyperfine coupling constants used for the simulation match well the calculated ones (Fig. 3). The spin density map shows that the highest spin density is at the carbon atom, where the σ-bond is formed between the monomeric units of the observed, most stable (c-**NC**)$_2$ σ-dimers. The neighboring carbon atom also shows a significant spin density, which makes the non-symmetric dimers plausible. An explanation as to why the isolated **HC** isomer is formed is that the oxidation of the non-symmetric dimer, non-sym-(*P**,*R**, *R**,*P**)-(c-**NC**)$_2$, which is higher in energy than the symmetric ones, has a smaller activation energy and proceeds faster than the oxidation of the symmetric dimers, which are in equilibrium with the non-symmetric one. In between (c-**NC**)$_2$ and **HC**, no further intermediates could be detected, indicating that the oxidation, EC, and second oxidation processes are fast.

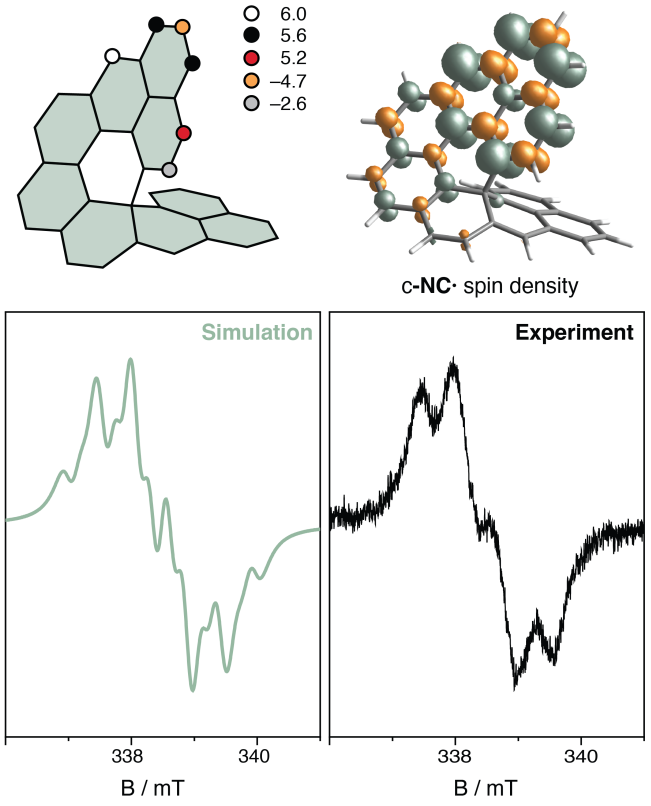

Figure 3. Experimental and simulated EPR spectrum and spin density of c-**NC**·. Hyperfine coupling constants that were used for the fitting are illustrated with colored dots.

Absorption and Emission. The absorption and emission spectra of **HC** were recorded in toluene at 20 °C (Fig. 4). The profile of the UV–vis absorption spectrum of **HC** shows high similarity to those of functionalized peropyrene derivatives reported in the literature[54,55], suggesting that the absorption properties arise mainly from the **PP** unit of **HC**. However, the solubility of **HC** is significantly higher than the **PP** solubility due to the contorted structure. For a comparison, *O*-c-**NC** absorbs mostly in the UV and not visible region. Similarly to absorption, the profile of the emission of **HC** also resembles that of **PP**. The fluorescence quantum yield (Φ_F) of **HC** in toluene is 0.45 (excitation at 470 nm, Fig. 5) with a Stokes shift of 60 meV. The Φ_F is lower by a factor of ~2 comparted to **PP**[56], which can be attributed to the out-of-plane twist[57–59] of the **PP** unit induced by strain from the locked helicene units. In comparison, *O*-c-**NC** shows a much larger Stokes shift of 840 meV, but a small Φ_F of 0.02, on account of quenching of the fluorescence by the carbonyl group.

Circular Dichroism (CD). The (*P*) and (*M*) enantiomers of **6** were separated by HPLC equipped with a chiral stationary phase (Fig. S6–S8), and the absolute configuration was assigned with the aid of CD spectra (Fig. S9) and TD-DFT calculations (Fig. S10) and optical rotation ($[\alpha]_D^{24.1}(P)$ = +4095°; $[\alpha]_D^{25.0}(M)$ = −4018°, lit.[60] (*P*)-[7]helicene: ~ +6000). In the CD spectra (Fig. S9), the enantiomers displayed mirror-image Cotton effects. The (*P*) enantiomer (>99% ee) of **6** was reduced and dehydrated to obtain the (*P*) enantiomer of 2*H*-**NC**. The reaction cascade with (*P*)-2*H*-**NC** afforded the corresponding (*P,P*)-**HC** and (*P*)-*O*-c-**NC** that were isolated. CD spectra for both compounds are shown in Figure 4 and match prediction by TD-DFT (Fig. S10–12).

Circularly Polarized Luminescence (CPL). Enantiomerically enriched (*P,P*)-**HC** showed good CPL response with an absorption dissymmetry factor g_{abs} = 1.13 × 10^{-3} at 502 nm. Interestingly, the luminescence dissymmetry factor has the same value g_{lum} = 1.13 × 10^{-3} at 520 nm. The g_{lum}/g_{abs} value as a measure of excited state relaxation for helicenes and helicenoids is typically ~0.6.[61,62] The deviation from unity is accounted for the flexibility of helicenes and helicenoids.[63] However, for (*P,P*)-**HC** the g_{lum}/g_{abs} value is precisely 1.0 suggesting high rigidity which is also expected with the two locked sp^3-centers. For better quantification of CPL emitter efficiency and better comparison B_{CPL} (brightness of CPL) was introduced as measuring quantity.[64] The CPL brightness for (*P,P*)-**HC** is 8.3 $M^{-1}cm^{-1}$ which is right at the median of reported [7]helicenes (including heteroatom containing helicenes).

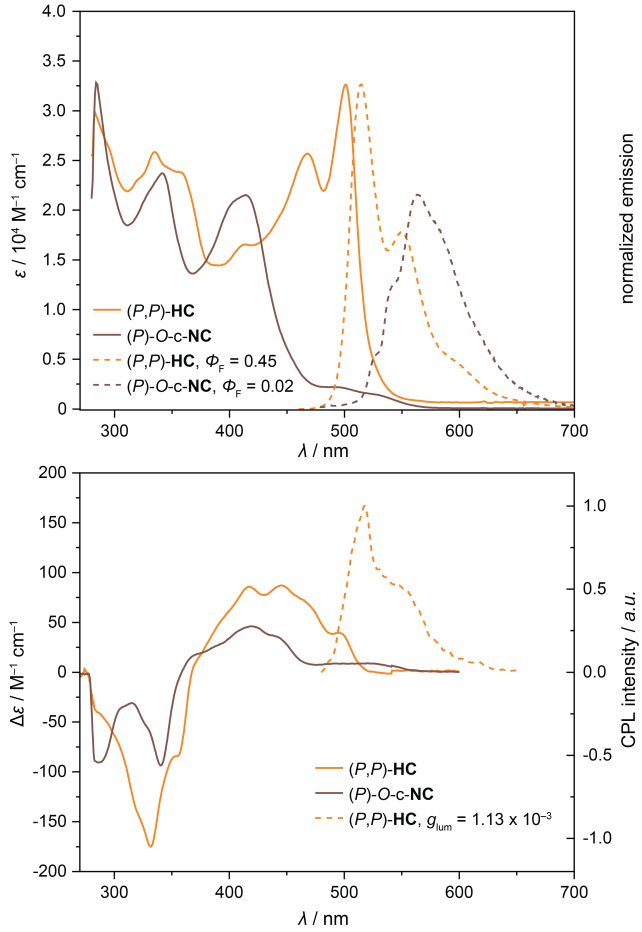

Figure 4. Absorption, emission (top), and circular dichroism, circularly polarized luminescence (bottom) spectra of enantioenriched (*P,P*)-**HC** and (*P*)-*O*-c-**NC** in toluene at 20 °C in toluene. Φ_F = quantum yield. g_{lum} = luminescence dissymmetry factor.

CONCLUSION

The research in the field of graphene-based π-radicals and π-radicaloids is primarily focused on the properties that arise from the presence of unpaired electrons in these open-shell molecules. When these molecules react, the unpaired electrons form bonds, which leads to the loss of the desired properties. Reactivity is therefore an unwanted element and synthetic strategies are developed to prevent it. When decomposition occurs, the pathways and byproducts are typically not investigated in depth, which makes an impression they are undefined. In this work, we demonstrated that reactivity of "unchained" diradicaloid molecules can be well-defined and has potential to become a useful synthetic tool to access warped carbon nanostructures via a series of multiple selective steps. The key

element of the presented cascade is the formation of a quaternary center—an "sp^3-defect"—during an electrocyclization or a radical ring-closing step, which locks the system from full fusion previously observed for cethrene. Upon oxidation, the system is activated for the second cascade round, analogous to oxidative dimerization of phenalenyl to peropyrene. The overall result is a sequence of up to nine steps, where four new σ- and one new π-bond are formed to give a conjugated contorted nanocarbon hypercethrene, containing two precisely installed sp^3-defects. By modulating the amount of oxidant, various intermediates of this cascade could be identified or even isolated and characterized. The photophysical properties of hypercethrene mostly resemble those of peropyrene, including its fluorescence with a quantum yield of 0.45. Resolution of enantiomers achieved via preparative chiral-stationary-phase HPLC made it possible to perform the reaction cascade with enantiomerically enriched (*P*) starting material. The isolated (*P,P*)-hypercethrene showed circular dichroism and circularly polarized luminescence with a CPL brightness value of 8.3 $M^{-1}cm^{-1}$. These results demonstrate that reactivity of unchained graphene-based π-radical(oid)s holds prospects to be explored in the future as a step-economic synthetic tool toward carbon nanostructures.

EXPERIMENTAL SECTION

Synthesis and Characterization. Experimental procedures and characterization data for all new compounds described in this work are compiled in the Supporting Information (sections S1–S8). Two routes **A** and **B** (Schemes S1 and S2) were followed to obtain 2*H*-c-**NC**. Since all characterizations were complete–and both routes were successful–we decided to report both routes. Overall, the number of steps does not change using one or the other approach. But the two-fold cyclization to obtain helicene **5** is not ideal due to partial loss of one or both bromides and their tedious separation from the desired helicene **5'**. Therefore, it was decided to install the carbon chain beforehand and perform said two-fold cyclization without bromides. Consequently, all carbon atoms for the **NC** scaffold are installed one step earlier. The linear synthetic sequence is shorter by converging the route. The second approach is also more scalable as the photocyclization step usually requires more diluted reaction conditions. The batch sizes are thus limited making this step the bottle neck of the synthesis. Shifting the photocyclization closer to the end in the synthetic pathway the bottle neck is less pronounced as batch sizes decrease.

All chemicals and solvents were purchased from commercial sources and were used without further purification unless stated otherwise. The reactions and experiments that are sensitive to dioxygen were performed using Schlenk techniques and nitrogen or argon-saturated solvents.

EPR spectroscopy. The electron paramagnetic resonance (EPR) spectra were recorded in N_2-saturated benzene on an X-band benchtop EPR spectrometer (9.48 GHz) using the following instrumental parameters: magnetic field 336–342 mT, scan time 1800 s, modulation amplitude 0.2 mT, microwave power 10 mW.

UV–vis, CD and Optical Rotation Spectroscopy. The specific optical rotation $[\alpha]_D^T$ (in ° mL dm^{-1} g^{-1}) was measured at an indicated temperature T (in °C) and a concentration c (in g/100 mL). Infrared spectra (IR) were recorded on an FT-IR ATR spectrophotometer applied as neat samples or as films; $1/\lambda$ in cm^{-1}. The UV-vis measurements were performed on an Agilent 8453 Spectrophotometer. Circular Dichroism (CD) spectra were recorded on a Jasco J-1000 Series CD Spectropolarimeter.

Fluorescence and CPL Spectroscopy. Experimental Fluorescence measurements were carried out using a calibrated Edinburgh Instruments FS5 spectrofluorometer equipped with an SC-25 Temperature Controlled Holder TE-Cooled-Standard cell for emission spectra and an SC-30 Integrating Sphere cell for obtaining quantum yields. All Samples were measured in quartz glass fluorescence cuvettes with 1 cm path length using spectroscopy grade solvents. CPL spectra were recorded with a customized JASCO CPL-300/J-1500 hybrid spectrometer.

NMR Spectroscopy and High Resolution Mass Spectrometry (HRMS). The NMR experiments were performed on NMR spectrometers operating at 400, 500, or 600 MHz proton frequencies. Standard pulse sequences were used. Chemical shifts (δ) are reported in parts per million (ppm) relative to the solvent residual peak (^{1}H and ^{13}C NMR, respectively): $CDCl_3$ (δ = 7.26 and 77.16 ppm[65]), CD_2Cl_2 (δ = 5.32 and 53.84 ppm[65]), and $C_2D_2Cl_4$ (δ = 6.00 and 73.78 ppm[66]). High-resolution mass spectra were measured as HR-EI-MS, HR-ESI-MS, or HR-APCI-MS.

Single-Crystal X-Ray Diffraction (XRD). All information about experimental setup, conditions, and software are compiled in the Supporting Information (sections S6). Suitable crystals of (*P*)-**6** for XRD were grown by slow evaporation from hexanes/CH_2Cl_2 solvent mixture. Suitable crystals of (*P*)-2*H*-**NC** for XRD were grown by slow evaporation from CH_3Cl. Suitable crystals of (±)-*O*-c-**NC** for XRD were grown by slow evaporation from heptane/toluene solvent mixture. Suitable crystals of (*P,S,R,M*)-(**NC**)$_2$ for XRD were grown by slow evaporation from oxygen-free benzene-d_6 in a NMR tube.

DFT Calculations. DFT calculations were performed using Gaussian 16 suite.[67] The multireference CASSCF calculations were performed using ORCA–4.2.1.[68] Geometries were optimized using ωB97XD functional and Def2SVP basis set in the gas phase. The frequency analysis was performed to verify the stationary state geometry, where no imaginary frequency was found. TD-DFT calculations were performed on ωB97XD/Def2SVP optimized geometries at the wB97XD/Def2SVP level. The effect of the solvent was accounted using PCM (with toluene as the solvent). SpecDis and Chemcraft software were used to analyze the TD-DFT calculated spectra and to generate graphical images of frontier molecular orbitals (FMOs), respectively.

For **NC** the singlet geometries were optimized with spin-restricted and spin-unrestricted broken-symmetry wavefunctions, whereas triplet geometry was optimized with spin-unrestricted wavefunctions. The restricted-singlet wavefunctions were tested for RHF→UHF instability. For the spin-restricted wavefunction RHF→UHF instability was found, which supports the open-shell singlet ground state for **NC**. The biradical character (0.9) was estimated using multireference CASSCF(2,2) calculation. The adiabatic singlet–triplet energy gap (0.17 kcal mol^{-1}) was calculated using CASSCF(2,2)/NEVPT2/def2-TZVPP approach on DFT optimized singlet and triplet geometries.

ASSOCIATED CONTENT

Supporting Information

The Supporting Information is available free of charge on the ACS Publications website.

Synthetic procedures and characterization data for all new compounds, UV–vis, HPLC, CD, EPR, XRD, and DFT calculation

details, assignment of ^{1}H and ^{13}C NMR resonances, copies of NMR and HRMS spectra, and Cartesian coordinates (PDF)

Accession Codes

CCDC 2157012 ((*P*)-**6**), 2157015 (2*H*-**NC**), 2157016 ((c-**NC**)$_2$), and 2157017 (*O*-c-**NC**) contain the supplementary crystallographic data for this paper. These data can be obtained free of charge via www.ccdc.cam.ac.uk/data_request/cif, or by emailing data_request@ccdc.cam.ac.uk, or by contacting The Cambridge Crystallographic Data Centre, 12 Union Road, Cambridge CB2 1EZ, UK; fax: +44 1223 336033.

AUTHOR INFORMATION

Corresponding Authors

Prince Ravat – *Institute of Organic Chemistry, University of Würzburg, 97074 Würzburg, Germany*;
https://orcid.org/0000-0002-7553-9188;
E-mail: princekumar.ravat@uni-wuerzburg.de

Michal Juríček – *Department of Chemistry, University of Zurich, 8057 Zurich, Switzerland*;
orcid.org/0000-0001-5595-431X;
E-mail: michal.juricek@chem.uzh.ch

Authors

Daniel Čavlović – *Department of Chemistry, University of Zurich, 8057 Zurich, Switzerland*; https://orcid.org/0000-0003-4057-6648

Daniel Häussinger – *Department of Chemistry, University of Basel, 4056 Basel, Switzerland*; https://orcid.org/0000-0002-4798-0072

Olivier Blacque – *Department of Chemistry, University of Zurich, 8057 Zurich, Switzerland*; orcid.org/0000-0001-9857-4042

Notes

The authors declare no conflict in interest.

ACKNOWLEDGMENT

This project received funding from the European Research Council (ERC) under the European Union's Horizon 2020 research and innovation programme (Grant Agreement No. 716139, M.J.), the Swiss National Science Foundation (SNSF, M.J./PZ00P2_148043, PP00P2_170534, and PP00P2_198900), and the Novartis University of Basel Excellence Scholarship (P.R. and M.J.). We thank Leoš Valenta for measuring EPR and Asim Kumar Swain for CPL measurements. We thank the University of Würzburg for ERC financial support within the "Excellent Ideas Programme". We thank Prof. Marcel Mayor for supporting our research at the University of Basel and Shaun O'Hare for suggesting the name hypercethrene.

REFERENCES

(1) Hu, X.; Wang, W.; Wang, D.; Zheng, Y. The Electronic Applications of Stable Diradicaloids: Present and Future. *Journal of Materials Chemistry C*. Royal Society of Chemistry November 1, 2018, pp 11232–11242. https://doi.org/10.1039/c8tc04484h.

(2) Zong, C.; Zhu, X.; Xu, Z.; Zhang, L.; Xu, J.; Guo, J.; Xiang, Q.; Zeng, Z.; Hu, W.; Wu, J.; Li, R.; Sun, Z. Isomeric Dibenzoheptazethrenes for Air-Stable Organic Field-Effect Transistors. *Angewandte Chemie International Edition* **2021**, *60* (29), 16230–16236. https://doi.org/10.1002/anie.202105872.

(3) Liu, J.; Feng, X. Synthetic Tailoring of Graphene Nanostructures with Zigzag-Edged Topologies: Progress and Perspectives. *Angewandte Chemie International Edition* **2020**, *59* (52), 23386–23401. https://doi.org/10.1002/anie.202008838.

(4) *Diradicaloids*, 1st ed.; Wu J.; Jenny Stanford Publishing, **2022**. ISBN 9781003277248.

(5) Abe, M. Diradicals. **2013**. https://doi.org/10.1021/cr400056a.

(6) Stuyver, T.; Chen, B.; Zeng, T.; Geerlings, P.; de Proft, F.; Hoffmann, R. Do Diradicals Behave like Radicals? *Chemical Reviews*. American Chemical Society November 13, 2019, pp 11291–11351. https://doi.org/10.1021/acs.chemrev.9b00260.

(7) Thiele, J.; Balhorn, H. Ueber Einen Chinoïden Kohlenwasserstoff. *Berichte der deutschen chemischen Gesellschaft* **1904**, *37* (2), 1463–1470. https://doi.org/10.1002/cber.19040370245.

(8) Montgomery, L. K.; Huffman, J. C.; Jurczak, E. A.; Grendze, M. P. The Molecular Structures of Thiele's and Chichibabin's Hydrocarbons. *Journal of the American Chemical Society* **1986**, *108* (19), 6004–6011. https://doi.org/10.1021/ja00279a056.

(9) Tschitschibabin, A. E. Über Einige Phenylierte Derivate Des *p* , *p* -Ditolyls. *Berichte der deutschen chemischen Gesellschaft* **1907**, *40* (2), 1810–1819. https://doi.org/10.1002/cber.19070400282.

(10) Ravat, P.; Baumgarten, M. "Tschitschibabin Type Biradicals": Benzenoid or Quinoid? *Physical Chemistry Chemical Physics* **2015**, *17* (2), 983–991. https://doi.org/10.1039/c4cp03522d.

(11) Müller, E.; Pfanz, H. Über Biradikaloide Terphenylderivate. *Berichte der deutschen chemischen Gesellschaft (A and B Series)* **1941**, *74* (6), 1051–1074. https://doi.org/10.1002/cber.19410740636.

(12) Zeng, Z.; Sung, Y. M.; Bao, N.; Tan, D.; Lee, R.; Zafra, J. L.; Lee, B. S.; Ishida, M.; Ding, J.; López Navarrete, J. T.; Li, Y.; Zeng, W.; Kim, D.; Huang, K. W.; Webster, R. D.; Casado, J.; Wu, J. Stable Tetrabenzo-Chichibabin's Hydrocarbons: Tunable Ground State and Unusual Transition between Their Closed-Shell and Open-Shell Resonance Forms. *Journal of the American Chemical Society* **2012**, *134* (35), 14513–14525. https://doi.org/10.1021/ja3050579.

(13) Ni, Y.; Gopalakrishna, T. Y.; Phan, H.; Herng, T. S.; Wu, S.; Han, Y.; Ding, J.; Wu, J. A Peri-Tetracene Diradicaloid: Synthesis and Properties. *Angewandte Chemie* **2018**, *130* (31), 9845–9849. https://doi.org/10.1002/ange.201804276.

(14) Shen, J.; Han, Y.; Dong, S.; Phan, H.; Herng, T. S.; Xu, T.; Ding, J.; Chi, C. A Stable [4,3]Peri-acene Diradicaloid: Synthesis, Structure, and Electronic Properties. *Angewandte Chemie International Edition* **2021**, *60* (9), 4464–4469. https://doi.org/10.1002/anie.202012328.

(15) Kubo, T.; Shimizu, A.; Uruichi, M.; Yakushi, K.; Nakano, M.; Shiomi, D.; Sato, K.; Takui, T.; Morita, Y.; Nakasuji, K. Singlet Biradical Character of Phenalenyl-Based Kekulé Hydrocarbon with Naphthoquinoid Structure. *Organic Letters* **2007**, *9* (1), 81–84. https://doi.org/10.1021/ol062604z.

(16) Kubo, T.; Shimizu, A.; Sakamoto, M.; Uruichi, M.; Yakushi, K.; Nakano, M.; Shiomi, D.; Sato, K.; Takui, T.; Morita, Y.; Nakasuji, K. Synthesis, Intermolecular Interaction, and Semiconductive Behavior of a Delocalized Singlet Biradical Hydrocarbon. *Angewandte Chemie International Edition* **2005**, *44* (40), 6564–6568. https://doi.org/10.1002/anie.200502303.

(17) Li, Y.; Huang, K. W.; Sun, Z.; Webster, R. D.; Zeng, Z.; Zeng, W.; Chi, C.; Furukawa, K.; Wu, J. A Kinetically Blocked 1,14:11,12-Dibenzopentacene: A Persistent Triplet Diradical of a Non-Kekulé Polycyclic Benzenoid Hydrocarbon. *Chemical Science* **2014**, *5* (5), 1908–1914. https://doi.org/10.1039/c3sc53015a.

(18) Shimizu, A.; Nobusue, S.; Miyoshi, H.; Tobe, Y. Indenofluorene Congeners: Biradicaloids and Beyond. In *Pure and Applied Chemistry*; IUPAC Secretariat, 2014; Vol. 86, pp 517–528. https://doi.org/10.1515/pac-2014-5043.

(19) Dressler, J. J.; Zhou, Z.; Marshall, J. L.; Kishi, R.; Takamuku, S.; Wei, Z.; Spisak, S. N.; Nakano, M.; Petrukhina, M. A.; Haley, M. M. Synthesis of the Unknown Indeno[1,2- a]Fluorene Regioisomer: Crystallographic Characterization of Its Dianion . *Angewandte Chemie* **2017**, *129* (48), 15565–15569. https://doi.org/10.1002/ange.201709282.

(20) Shimizu, A.; Tobe, Y. Indeno[2,1-a]Fluorene: An Air-Stable Ortho-Quinodimethane Derivative. *Angewandte Chemie International Edition* **2011**, *50* (30), 6906–6910. https://doi.org/10.1002/anie.201101950.

(21) Sahara, K.; Abe, M.; Zipse, H.; Kubo, T. Duality of Reactivity of a Biradicaloid Compound with an O-Quinodimethane Scaffold. *Journal of the American Chemical Society* **2020**, *142* (11), 5408–5418. https://doi.org/10.1021/jacs.0c01003.

(22) Hu, P.; Lee, S.; Park, K. H.; Das, S.; Herng, T. S.; Gonçalves, T. P.; Huang, K. W.; Ding, J.; Kim, D.; Wu, J. Octazethrene and Its Isomer with Different Diradical Characters and Chemical Reactivity: The Role of the Bridge Structure. *Journal of Organic Chemistry* **2016**, *81* (7), 2911–2919. https://doi.org/10.1021/acs.joc.6b00172.

(23) Zeng, W.; Sun, Z.; Herng, T. S.; Gonçalves, T. P.; Gopalakrishna, T. Y.; Huang, K.-W.; Ding, J.; Wu, J. Super-Heptazethrene. *Angewandte Chemie International Edition* **2016**, *55* (30), 8615–8619. https://doi.org/10.1002/anie.201602997.

(24) Li, Y.; Heng, W. K.; Lee, B. S.; Aratani, N.; Zafra, J. L.; Bao, N.; Lee, R.; Sung, Y. M.; Sun, Z.; Huang, K. W.; Webster, R. D.; López Navarrete, J. T.; Kim, D.; Osuka, A.; Casado, J.; Ding, J.; Wu, J. Kinetically Blocked Stable Heptazethrene and Octazethrene: Closed-Shell or Open-Shell in the Ground State? *Journal of the American Chemical Society* **2012**, *134* (36), 14913–14922. https://doi.org/10.1021/ja304618v.

(25) Ravat, P.; Tomáš, T.; Olomek, S.̌; Hä, D.; Blacque, O.; Juríč, M. Dimethylcethrene: A Chiroptical Diradicaloid Photoswitch. *J. Am. Chem. Soc* **2018**, *140*, 10839–10847. https://doi.org/10.1021/jacs.8b05465.

(26) Ravat, P.; Šolomek, T.; Rickhaus, M.; Häussinger, D.; Neuburger, M.; Baumgarten, M.; Juríček, M. Cethrene: A Helically Chiral Biradicaloid Isomer of Heptazethrene. *Angewandte Chemie - International Edition* **2016**, *55* (3), 1183–1186. https://doi.org/10.1002/anie.201507961.

(27) Konishi, A.; Kubo, T. Benzenoid Quinodimethanes. *Topics in Current Chemistry*. Springer International Publishing December 1, 2017. https://doi.org/10.1007/s41061-017-0171-2.

(28) Pogodin, S.; Agranat, I. Biphenalenylidene: The Forgotten Bistricyclic Aromatic Ene. A Theoretical Study. *Journal of the American Chemical Society* **2003**, *125* (42), 12829–12835. https://doi.org/10.1021/ja035968k.

(29) Menon, A.; Martin, J. W.; Akroyd, J.; Kraft, M. Reactivity of Polycyclic Aromatic Hydrocarbon Soot Precursors: Kinetics and Equilibria. *Journal of Physical Chemistry A* **2020**, *124* (48), 10040–10052. https://doi.org/10.1021/acs.jpca.0c07811.

(30) Hu, P.; Lee, S.; Herng, T. S.; Aratani, N.; Gonçalves, T. P.; Qi, Q.; Shi, X.; Yamada, H.; Huang, K. W.; Ding, J.; Kim, D.; Wu, J. Toward Tetraradicaloid: The Effect of Fusion Mode on Radical Character and Chemical Reactivity. *Journal of the American Chemical Society* **2016**, *138* (3), 1065–1077. https://doi.org/10.1021/jacs.5b12532.

(31) Valenta, L.; Mayländer, M.; Kappeler, P.; Blacque, O.; Šolomek, T.; Richert, S.; Juríček, M. Trimesityltriangulene: A Persistent Derivative of Clar's Hydrocarbon. *Chemical Communications* **2022**. https://doi.org/10.1039/D2CC00352J.

(32) Arikawa, S.; Shimizu, A.; Shiomi, D.; Sato, K.; Shintani, R. Synthesis and Isolation of a Kinetically Stabilized Crystalline Triangulene. *Journal of the American Chemical Society* **2021**, *143* (46), 19599–19605. https://doi.org/10.1021/jacs.1c10151.

(33) Juríček, M. The Three c's of Cethrene. *Chimia* **2018**, *72* (5), 322–327. https://doi.org/10.2533/chimia.2018.322.

(34) Čavlović, D.; Juríček, M. Molecular Magnetic Switches. In *Chimia*; Swiss Chemical Society, 2019; Vol. 73, pp 313–316. https://doi.org/10.2533/chimia.2019.313.

(35) Ravat, P.; Šolomek, T.; Juríček, M. Helicenes as Chiroptical Photoswitches. *ChemPhotoChem* **2019**, *3* (4), 180–186. https://doi.org/10.1002/cptc.201800229.

(36) Wonink, M. B. S.; Corbet, B. P.; Kulago, A. A.; Boursalian, G. B.; de Bruin, B.; Otten, E.; Browne, W. R.; Feringa, B. L. Three-State Switching of an Anthracene Extended Bis-Thiaxanthylidene with a Highly Stable Diradical State. *Journal of the American Chemical Society* **2021**, *143* (43), 18020–18028. https://doi.org/10.1021/jacs.1c05938.

(37) Nishiuchi, T.; Ito, R.; Stratmann, E.; Kubo, T. Switchable Conformational Isomerization of an Overcrowded Tristricyclic Aromatic Ene. *Journal of Organic Chemistry* **2020**, *85* (1), 179–186. https://doi.org/10.1021/acs.joc.9b02432.

(38) Yang, Y.; Huangfu, S.; Sato, S.; Juríč, M. Cycloparaphenylene Double Nanohoop: Structure, Lamellar Packing, and Encapsulation of C 60 in the Solid State. *Org. Lett* **2021**, *23*, 41. https://doi.org/10.1021/acs.orglett.1c02950.

(39) Yang, Y.; Blacque, O.; Sato, S.; Juríček, M. Cycloparaphenylene–Phenalenyl Radical and Its Dimeric Double Nanohoop**. *Angewandte Chemie* **2021**, *133* (24), 13641–13647. https://doi.org/10.1002/ange.202101792.

(40) Šolomek, T.; Ravat, P.; Juríček, M. 'Forbidden' Electrocyclizations of Diradicaloids. *Trends in Chemistry*. Cell Press October 1, 2019, pp 705–706. https://doi.org/10.1016/j.trechm.2019.08.005.

(41) Šolomek, T.; Ravat, P.; Mou, Z.; Kertesz, M.; Juríček, M. Cethrene: The Chameleon of Woodward-Hoffmann Rules. *Journal of Organic Chemistry* **2018**, *83* (8), 4769–4774. https://doi.org/10.1021/acs.joc.8b00656.

(42) Uchida, K.; Ito, S.; Nakano, M.; Abe, M.; Kubo, T. Biphenalenylidene: Isolation and Characterization of the Reactive Intermediate on the Decomposition Pathway of Phenalenyl Radical. *Journal of the American Chemical Society* **2016**, *138* (7), 2399–2410. https://doi.org/10.1021/jacs.5b13033.

(43) Note: Such a switch was reported recently. However, the operating temperatures of this example are cryogenic. Günther, K.; Grabicki, N.; Battistella, B.; Grubert, L.; Dumele, O. *An All-Organic Photochemical Magnetic Switch with Bistable Spin States*; 2022. https://doi.org/10.26434/CHEMRXIV-2022-BH283.

(44) Li, C. le; Shieh, S. J.; Lin, S. C.; Liu, R. S. Synthesis and Spectroscopic Properties of Finite Ph 2N-Containing Oligo(Arylenevinylene) Derivatives That Emit Blue to Red Fluorescence. *Organic Letters* **2003**, *5* (7), 1131–1134. https://doi.org/10.1021/ol034246v.

(45) Jeong, K. S.; Kim, S. Y.; Shin, U. S.; Kogej, M.; Hai, N. T. M.; Broekmann, P.; Jeong, N.; Kirchner, B.; Reiher, M.; Schalley, C. A. Synthesis of Chiral Self-Assembling Rhombs and Their Characterization in Solution, in the Gas Phase, and at the Liquid-Solid Interface. *Journal of the American Chemical Society* **2005**, *127* (50), 17672–17685. https://doi.org/10.1021/ja053781i.

(46) Note: The Lithium–Halogen Exchange Can Also Be Achieved with n-Butyllithium Instead of Tert-Butyllithium, However, High-Er Temperatures and Longer Reaction Times Are Required to Achieve Comparable Yields Compared to the Use of Tert-Butyllithium.
(47) Note: All Cis/Trans Isomers Obtained in the Wittig Reaction Give the Same Product in the Photocyclodehydrogenation Step. Therefore, Only a Small Quantity of 4 Was Isomerized to Thermodynamically the Most Stable Trans,Trans Product for Structural Characterization Purposes.
(48) Note: Initial Attempts with Different Lewis Acids Resulted in Lower Conversions. The Friedel–Crafts Reaction Does Not Work below −55 °C. Only above This Temperature, a Color Change and Conversion of the Starting Material Is Observed.
(49) Ravat, P.; Ribar, P.; Rickhaus, M.; Häussinger, D.; Neuburger, M.; Juríček, M. Spin-Delocalization in a Helical Open-Shell Hydrocarbon. *Journal of Organic Chemistry* **2016**, *81* (24), 12303–12317. https://doi.org/10.1021/acs.joc.6b02246.
(50) Note: The Stereogenic Centers of the Helicenes Are Assigned More Reader Friendly with P and M to Minimize Confusion of Changing Priorities for Easier Understanding.
(51) Note: The Sym-(c-NC)2 Possesses 10 While the Non-Sym-(c-NC)2 Has 12 Possible Stereoisomers.
(52) Mou, Z.; Uchida, K.; Kubo, T.; Kertesz, M. Evidence of σ- And π-Dimerization in a Series of Phenalenyls. *Journal of the American Chemical Society* **2014**, *136* (52), 18009–18022. https://doi.org/10.1021/ja509243p.
(53) Zhang, R.; Ellern, A.; Winter, A. H. Steric Hindrance Favors σ Dimerization over π Dimerization for Julolidine Dicyanomethyl Radicals. *Journal of Organic Chemistry* **2022**, *87* (2), 1507–1511. https://doi.org/10.1021/acs.joc.1c02246.
(54) Yang, W.; Monteiro, J. H. S. K.; de Bettencourt-Dias, A.; Catalano, V. J.; Chalifoux, W. A. Pyrenes, Peropyrenes, and Teropyrenes: Synthesis, Structures, and Photophysical Properties. *Angewandte Chemie International Edition* **2016**, *55* (35), 10427–10430. https://doi.org/10.1002/anie.201604741.
(55) Uchida, K.; Kubo, T.; Yamanaka, D.; Furube, A.; Matsuzaki, H.; Nishii, R.; Sakagami, Y.; Abulikemu, A.; Kamada, K. Synthesis, Crystal Structure, and Photophysical Properties of 2,9-Disubstituted Peropyrene Derivatives. *Canadian Journal of Chemistry* **2017**, *95* (4), 432–444. https://doi.org/10.1139/cjc-2016-0569.
(56) Nichols, V. M.; Rodriguez, M. T.; Piland, G. B.; Tham, F.; Nesterov, V. N.; Youngblood, W. J.; Bardeen, C. J. Assessing the Potential of Peropyrene as a Singlet Fission Material: Photophysical Properties in Solution and the Solid State. *Journal of Physical Chemistry C* **2013**, *117* (33), 16802–16810. https://doi.org/10.1021/jp4051116.
(57) Lin, C. T.; Stikeleather, J. A. The Effect of Molecular Distortion in the Rates of Intersystem Crossing S1 {A Figure Is Presented} Tx {A Figure Is Presented} S0 Processes. *Chemical Physics Letters* **1976**, *38* (3), 561–566. https://doi.org/10.1016/0009-2614(76)80040-1.
(58) Malakar, P.; Borin, V.; Bedi, A.; Schapiro, I.; Gidron, O.; Ruhman, S. The Impact of Twisting on the Intersystem Crossing in Acenes: An Experimental and Computational Study. *Physical Chemistry Chemical Physics* **2022**, *24* (4), 2357–2362. https://doi.org/10.1039/d1cp05728f.
(59) Yang, W.; Longhi, G.; Abbate, S.; Lucotti, A.; Tommasini, M.; Villani, C.; Catalano, V. J.; Lykhin, A. O.; Varganov, S. A.; Chalifoux, W. A. Chiral Peropyrene: Synthesis, Structure, and Properties. *Journal of the American Chemical Society* **2017**, *139* (37), 13102–13109. https://doi.org/10.1021/jacs.7b06848.
(60) Nakai, Y.; Mori, T.; Inoue, Y. Theoretical and Experimental Studies on Circular Dichroism of Carbo[n]Helicenes. *Journal of Physical Chemistry A* **2012**, *116* (27), 7372–7385. https://doi.org/10.1021/jp304576g.
(61) Tanaka, H.; Inoue, Y.; Mori, T. Circularly Polarized Luminescence and Circular Dichroisms in Small Organic Molecules: Correlation between Excitation and Emission Dissymmetry Factors. *ChemPhotoChem* **2018**, *2* (5), 386–402. https://doi.org/10.1002/cptc.201800015.
(62) Swain, A. K.; Radacki, K.; Braunschweig, H.; Ravat, P. Pyrene-Fused [7]Helicenes Connected Via Hexagonal and Heptagonal Rings: Stereospecific Synthesis and Chiroptical Properties. *Journal of Organic Chemistry* **2022**, *87* (2), 993–1000. https://doi.org/10.1021/acs.joc.1c02281.
(63) Tanaka, H.; Ikenosako, M.; Kato, Y.; Fujiki, M.; Inoue, Y.; Mori, T. Symmetry-Based Rational Design for Boosting Chiroptical Responses. *Communications Chemistry* **2018**, *1* (1), 1–8. https://doi.org/10.1038/s42004-018-0035-x.
(64) Arrico, L.; di Bari, L.; Zinna, F. Quantifying the Overall Efficiency of Circularly Polarized Emitters. *Chemistry – A European Journal* **2021**, *27* (9), 2920–2934. https://doi.org/10.1002/chem.202002791.
(65) Fulmer, G. R.; Miller, A. J. M.; Sherden, N. H.; Gottlieb, H. E.; Nudelman, A.; Stoltz, B. M.; Bercaw, J. E.; Goldberg, K. I. NMR Chemical Shifts of Trace Impurities: Common Laboratory Solvents, Organics, and Gases in Deuterated Solvents Relevant to the Organometallic Chemist. *Organometallics* **2010**, *29* (9), 2176–2179. https://doi.org/10.1021/om100106e.
(66) O'Neil, M. J.; Heckelman, P. E.; Koch, C. B.; Roman, K. J. *The Merck Index, an Encyclopedia of Chemicals, Drugs, and Biologicals*; Merck Co.: Inc. Whitehouse Station, NJ, 2006.
(67) Frisch, M. J.; Trucks, G. W.; Schlegel, H. B.; Scuseria, G. E.; Robb, M. A.; Cheeseman, J. R.; Scalmani, G.; Barone, V.; Petersson, G. A.; Nakatsuji, H.; Li, X.; Caricato, M.; Marenich, A. v.; Bloino, J.; Janesko, B. G.; Gomperts, R.; Mennucci, B.; Hratchian, H. P.; Ortiz, J. v.; Izmaylov, A. F.; Sonnenberg, J. L.; Williams-Young, D.; Ding, F.; Lipparini, F.; Egidi, F.; Goings, J.; Peng, B.; Petrone, A.; Henderson, T.; Ranasinghe, D.; Zakrzewski, V. G.; Gao, J.; Rega, N.; Zheng, G.; Liang, W.; Hada, M.; Ehara, M.; Toyota, K.; Fukuda, R.; Hasegawa, J.; Ishida, M.; Nakajima, T.; Honda, Y.; Kitao, O.; Nakai, H.; Vreven, T.; Throssell, K.; Montgomery, J. A. , Jr.; Peralta, J. E.; Ogliaro, F.; Bearpark, M. J.; Heyd, J. J.; Brothers, E. N.; Kudin, K. N.; Staroverov, V. N.; Keith, T. A.; Kobayashi, R.; Normand, J.; Raghavachari, K.; Rendell, A. P.; Burant, J. C.; Iyengar, S. S.; Tomasi, J.; Cossi, M.; Millam, J. M.; Klene, M.; Adamo, C.; Cammi, R.; Ochterski, J. W.; Martin, R. L.; Morokuma, K.; Farkas, O.; Foresman, J. B.; Fox, D. J. Gaussian 16 Rev. C.01. Wallingford, CT 2016.
(68) Neese, F.; Wennmohs, F.; Becker, U.; Riplinger, C. The ORCA Quantum Chemistry Program Package. *Journal of Chemical Physics* **2020**, *152* (22), 224108. https://doi.org/10.1063/5.0004608.